Low-cycle fatigue crack initiation and propagation from controlled surface imperfections in nuclear steels

Paul Cussac, Catherine Gardin, Véronique Pelosin, Gilbert Hénaff, Laurent de Baglion, Olivier Ancelet, Stéphan Courtin

Low-cycle fatigue crack initiation and propagation from controlled surface imperfections in nuclear steels

International Journal of Fatigue, 2020, 139 : 105703

Cussac, P., C. Gardin, V. Pelosin, G. Hénaff, L. de Baglion, O. Ancelet, and S. Courtin

Abstract

The impact of a controlled surface imperfection on the low-cycle fatigue life in two different steels used in the French nuclear industry (304L austenitic stainless steel and 18MND5 low alloy steel) is investigated. After introduction of a single imperfection with a straight front and a depth varying from 50 to 350 µm in cylindrical samples, fatigue tests were conducted under fully-reversed total axial strain control in air at ambient temperature. It is shown that the fatigue life is significantly reduced, even in presence of small imperfections. In addition, the use of the potential drop methods provided an assesment of the initiation life and the determination of crack growth rates. Two characteristic crack growth domains were thus identified.

Corresponding author : catherine.gardin@ensma.fr

Keywords : Austenitic stainless steel; low-alloy steel; low-cycle fatigue; surface imperfection; fatigue life

Nomenclature

a	crack depth
a/b	ellipticity ratio or shape factor
b	ellipsis semi-major axis
D	specimen diameter
a/D	normalized crack depth
$\Delta\varepsilon_t$	total strain amplitude
DCPD	Direct Current Potential Drop
EDM	Electro Discharge Machining
N	lifetime in number of cycles
V	electrical potential difference
V_0	maximum value of V at the first cycle
V/V_0	normalized electrical potential difference

1. Introduction

Given the stringent requirements of high levels of safety in nuclear components, stakeholders of the French nuclear industry must anticipate the potential occurrence of residual surface imperfections and justify the residual resistance of the concerned parts, in particular under cyclic loading. The surface anomalies considered in this context may be introduced at the end of manufacturing operations (finishing, marking, non-destructive testing) or during handling steps. Indeed, during these operations, surface defects, with a depth of a few tenths of a millimeter, can be generated during undesired events such as tool fall or friction, or during required and controlled operations, such as the positioning of slings. Generally, surface imperfections can act as initiation sites and as a consequence can affect the fatigue strength [1-4]. The issue of the fatigue strength of metal components in the presence of surface anomalies

has been the subject of a relatively large number of studies, but mainly in the high-cycle fatigue regime [1, 3, 5]. For instance Inchekel and Talia [5] have studied the influence of scratches on the fatigue resistance of an Al-Li alloy and have shown that their presence is highly detrimental with a lifetime reduction close to 90% compared to those obtained on plain specimens. Cini and Irving [3] have reached similar conclusions by studying the impact of the presence of scratches on aluminium foil surfaces. They furthermore highlighted the influence of geometrical parameters such as the scratch depth or root radius. A more recent study [1] has assessed the effect of several types of surface imperfection on fatigue life in a nickel-base superalloy. These authors more particularly evidenced the major influence of residual stresses generated during the introduction of surface imperfections such as dents or scratches.

One of the major differences of the present sudy with respect to literature is that it is concerned with low-cycle fatigue instead of high-cycle fatigue. Indeed, in addition to the thermal fluctuations resulting from usual operating conditions, which are associated with stress amplitudes below the fatigue limit, higher stresses can appear during transients. Such transients, which correspond to power changes or unit start and restart, can generate thermal shocks associated with large deformations inducing yielding.

The fatigue strength under large-scale plasticity in steels used in the nuclear industry has been widely studied. Recent studies on 304L austenitic stainless steel have in particular adressed the sensitivity of its fatigue resistance to various parameters such as the environment [6], the loading type [7] or the surface finish [8-9]. For example, Poulain [8] has studied the effect of a ground surface finish and has put forward that the induced surface roughness can not only affect crack initiation, but also the first stages of propagation. Nevertheless, the impact of the presence of a unique surface imperfection similar in shape to unintentionally generated scratches or dent, under large-scale yielding conditions, has not been received a large attention so far on this type of material.

The present study was undertaken in order to get a first assesment of the effect of surface imperfections on the low-cycle fatigue resistance by considering two grades of steel typically used in French nuclear power plants, namely an austenitic stainless steel 304L and a low-alloy steel 18MND5 (equivalent to A533B). The selection of these two grades was supported by the fact that the low-cycle fatigue of 304L is well documented in the authors groups, while it also seemed interesting to conduct the same investigation in a grade with radically different properties for comparison purposes. Besides, the surface imperfections considered here have to be as close as possible from actual imperfections, that means characterized by a straigth front, a depth ranging between 100 and 350 µm, and a moderate notch root radius. However, for the sake of conservatism of the approach, it was also decided not to take advantage of the possible beneficial effect of compressive stresses which can be generated during the introduction of an initial flaw like an impact or a scratch [1-2]. A special attention has thus been paid to develop an experimental procedure to introduce surface imperfections that have to be reproducible, representative of actual imperfections, free of residual stresses while giving rise to crack initiation and propagation. With this aim, uniaxial low-cycle fatigue tests have been conducted under total strain amplitude control on cylindrical samples containing an imperfection. In addition, during the fatigue tests, the crack initiation and crack propagation stages have been monitored by use of the direct current potential drop method (DCPD). This method requires the prior determination of a calibration curve relating the potential measurements to the crack depth and the reliability of the method strongly depends on the accuracy of this calibration. While

many techniques exist to calibrate the electrical potential evolution during crack propagation, namely analytical [10-11] , analogical [10,12], numerical [13-16] and experimental [15, 17, 18], in this study, an experimental calibration based on the use of ink markings has been established.

After a presentation of the aforementioned experimental methods, the low-cycle fatigue results results obtained in both 304L and 18MND5 steels are detailed. The crack initiation and propagation aspects are addressed.

2. Materials and experimental methods

2.1. Materials description

A 304L austenitic stainless steel and a low-alloy 18MND5 steel, respectively used for the primary circuit pipes and the steam generators of the French nuclear power plants, have been studied here. The 304L samples have been taken from a sheet obtained by rolling and having undergone heat treatment at 1100°C followed by quenching with water. This treatment guarantees the austenitic phase homogeneity at ambient temperature. The chemical composition is given in table 1. The microstructure consists of an austenitic matrix dotted with residual ferrite lamellas. The average size of grains is about 80 µm [19, 20].

Element	C	Cr	Ni	Si	Mn	S	P	Mo	Cu	N
Content (%)	0.029	18.00	10.0	0.37	1.86	0.004	0.029	0.04	0.02	0.056

Table 1 – 304L chemical composition [21]

The 18MND5 specimens have been taken from a steam generator shell section. The chemical composition is given in table 2. Its good mechanical properties are due to the main following alloying elements: manganese, nickel and molybdenum. The microstructure, of bainitic type, consists of ferrite laths and carbides (cementite and molybdenum carbides). The prior austenite grain size is close to 20 µm.

Element	C	Mn	Ni	Mo	Cr	Si	Cu	Al	V	S	P
Content (%)	0.18	1.55	0.71	0.5	0.16	0.21	0.04	0.02	0.02	0.001	0.007

Table 2 – 18MND5 chemical composition

2.2. Specimen geometry and fatigue tests

For both materials, the specimens have been machined by wire Electro-Discharge Machining (EDM) and in such a way that the longitudinal axis of the specimens coincided with the rolling direction for the 304L and the longitudinal steam generator shell axis for the 18MND5. The specimens have a cylindrical shape with a 9 mm diameter and a 13.5 mm gauge length, as shown in figure 1. All the specimens have been mirror-polished prior to testing in order to unambiguously evidence the influence of surface imperfections.

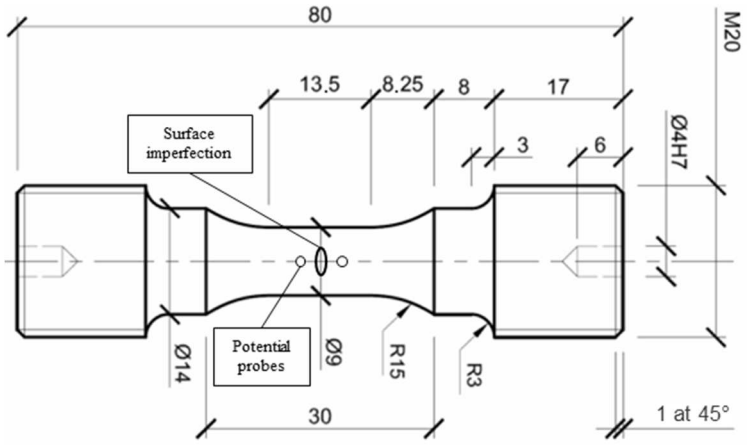

Figure 1 – Specimen geometry with surface imperfection and potential probes location

All the tests have been carried out at room temperature in laboratory air and under total strain amplitude control with a strain ratio $R_\varepsilon = -1$. Strain was controlled using a remote extensometer with ceramic rods. Three strain amplitudes have been considered: $\Delta\varepsilon_t / 2 = 0.2\%$, $\Delta\varepsilon_t / 2 = 0.3\%$ and $\Delta\varepsilon_t / 2 = 0.6\%$. All the tests have been conducted on an Instron electromechanical fatigue machine equipped with a static 100 kN capacity load cell and adapted to cyclic load variations between -50 and +50 kN. The applied strain rate was kept constant and set at 0.4% $\times s^{-1}$. The resulting frequencies then varied between 0.167 and 0.5 Hz, depending on the strain amplitude considered. The tests are stopped on the basis of a load drop criteria, the lifetimes considered in the framework of this study are associated with a 5% drop in the stabilized stress and are noted N_5.

Most of the tests have been carried out on specimens containing a surface imperfection. A unique imperfection was introduced per specimen. The imperfection was systematically placed in the center of the specimen gauge (figure 1) and perpendicular to the stress axis, so as to introduce a mode I loading for the crack initiated from the imperfection, which is recognized as being the most unfavorable case for fatigue crack growth.

2.3. Introduction of the surface imperfections

Two methods have been used for machining surface imperfections:

- A sinker electro-discharge machining (EDM) process based on the use of electrodes made of copper and designed to obtain sharp artificial notches;

- An “abrasive machine” which has been developed by the Pprime Institute in the context of previous studies [1,16] and which consists in a gradual removal of material by abrasion using a ceramic disc and a diamond powder. In order to get sharp imperfections like those introduced by the EDM method, the abrasive machine disk is previously sharpened.

The choice of these two processes is related, first, to the good geometrical reproductibility of the surface imperfections obtained but also, as we care about conservatism, to the need to limit the compressive residual stresses at the bottom of the imperfections. Actually, it is well known that this kind of stress generally delays crack initiation and propagation [1-2]. The imperfections artificially introduced in this study cover a range of depths from approximately 50 to 350 μm. Geometric characteristics of all the imperfections have been systematically analyzed by means of an optical microscope. The imperfection length and width depend on the depth and vary

respectively from approximately 1.5 to 3.5 mm and from 200 to 400 µm. The average opening angle and notch root radius are respectively 40° and 80 µm.

2.4. Crack initiation and growth monitoring : DCPD technique and ink markings

The Direct Current Potential Drop monitoring method, also known as DCPD, was implemented to monitor the initiation and propagation of cracks during tests. It consists in introducing a direct current through a specimen and in measuring the potential value on both sides of the crack. During crack growth, the electrical resistance rises and causes, in accordance with Ohm's law, an increase in the potential difference between the measurement points. It is then possible to monitor in real-time the crack growth. The use of this technique has been possible thanks to the damage localization induced by the presence of the surface imperfection. Indeed, the implementation of potential monitoring requires the prior knowledge of the crack initiation location in order to place the potential probes. In this study, the main crack has systematically initiated from artificially introduced surface defects. The electrical current is introduced into the samples by means of wires connected to the machine grip lines. The latter has been previously isolated from the rest of the machine frame by means of insulating sheets to prevent electrical interference and to limit the noise in the potential signal. In order to reduce the specimen heating by Joule effect, which could influence the potential measurement, the current is introduced per pulse (I_{min} = 0 and I_{max} = 1 A) at a 100 Hz frequency. The electrical voltage, denoted V, is measured by means of 0.1 mm diameter platinum wires which are spot-welded at a distance of 1 mm from the defect center. In order to ensure that the measurement is independent of material properties, V is normalized using the value measured at the first cycle maximum, denoted V_0. This formalism also enables to take into account the plastic deformation occurring at the beginning of the test and which may influence the measurement of the potential [22-24].

However, this technique requires to determine a reliable calibration curve connecting the measured potential difference to the crack depth.

The ink marking technique has been selected to visualize the crack fronts at different steps during propagation. This technique is inexpensive and easy to implement, and it furthermore gives satisfying results in the conditions examined here (tests in laboratory air at room temperature). The inks used are fast-drying acrylic and are commercially purchased. By the use of different ink colors during a test, several markings can be performed on the same fracture surface.

The principle of this method is to apply ink directly on the specimen surface near the surface imperfection by using a brush. This very fast operation is followed by a phase of removal of the ink in excess at the surface. The markings are realized without stopping the tests, allowing a better ink penetration during the crack opening phase. The operation is carried out during a few cycles only (between 2 and 10 approximately, depending on the test frequency) and the rapid drying of the ink limits its spread after application.

3. Experimental results

3.1. Calibration of the Direct Current Potential Drop method

3.1.1. Crack initiation threshold

One of the first challenges in calibrating electrical potential monitoring is to be able to identify a threshold above which a crack initiated from the initial imperfection is assumed to propagate. In order to evidence an initiation threshold, several markings were made on 304L specimens, for different relative values of the electrical potential difference. The analysis of these markings according to the applied strain or the initial imperfection depth has shown that those parameters have no significant influence on the initiation threshold. The ink markings performed on 304L steel have revealed that a 1% variation in the normalized potential difference can be associated with a crack depth close to 100 µm. One ink marking performed onto a 18MND5 sample (figure 2) has confirmed this value. Consequently, the 1% potential variation has been considered as the threshold for crack initiation in both materials in the subsequent tests. This initiation threshold definition has been subsequently used to analyze experimental data resulting from fatigue tests. One can note that it is consistent with the grain size in 304L which is close to 80 µm on average. This order of magnitude for the initiation threshold (100 µm depth) has been used by some authors [1,25].

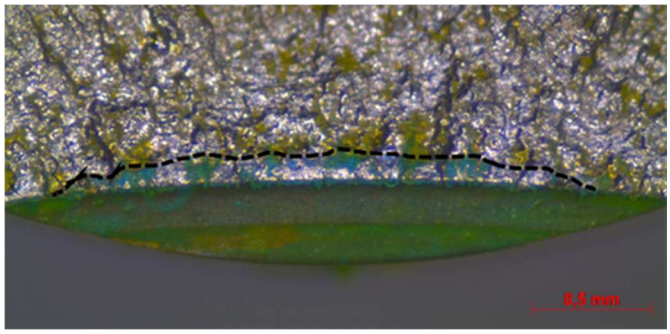

Figure 2 - Ink marking in a 18MND5 specimen associated with a crack propagation close to 100 µm in depth

3.1.2. Calibration of the electric potential method

The experimental calibration of the electrical potential crack growth monitoring is based on the observation of the fracture surfaces after completion of the fatigue tests. The use of a relatively large number of ink markings permitted to characterize the propagation. Indeed, based on these markings but also on the final crack fronts, it is possible to observe several crack propagation stages on the same fracture surface. All the collected information was used, by associating each marking and crack front with a given experimental potential value, to experimentally reconstruct the crack depth variation as a function of the potential difference evolution as shown in figure 3. Experimental data generated for both materials are represented on this curve without distinction of the test conditions in terms of applied strain amplitude or initial notch geometry. Furthermore the crack depth value considered in this figure is the maximum depth at the center of the test sample by taking as a reference the notch root (a_i in figure 7). In other words, only the propagated part of the crack is taken into account here.

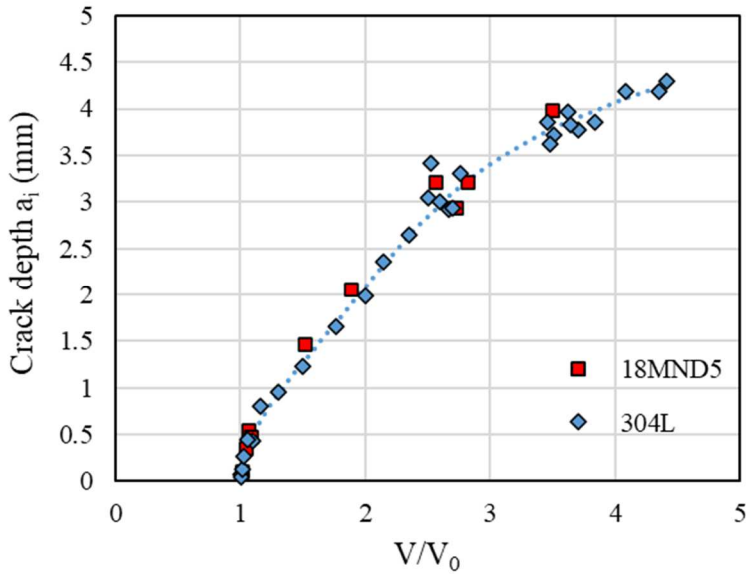

Figure 3 - Crack depth as a function of the normalized potential difference for both 304L and 18MND5 steels.

No influence of the various test parameters can be noticed here. Hence, the total strain amplitude, the initial surface imperfection depth or the material do not affect the electrical potential variation in the framework of this study. This result can be partly explained by the use of a reference potential V_0 which, in particular, allows to get free of the material electric properties. In order to use the calibration data continuously, an interpolation of the 304L data was performed (dashed line in figure 3).

3.2. Crack initiation from surface imperfection

3.2.1. Crack initiation observations

In fatigue tests carried out on specimens containing a surface imperfection, the initiation of the main crack systematically occurred from this imperfection. More specifically, whatever the strain level or the imperfection depth and type considered, optical observations carried out during the tests by means of a long focal length microscope, have revealed a systematic initiation in the center and at the root of the defects. These zones correspond to the maximum surface imperfection depth and are associated with a significant deformation concentration. An example of a crack initiated at an imperfection root is shown in figure 4.

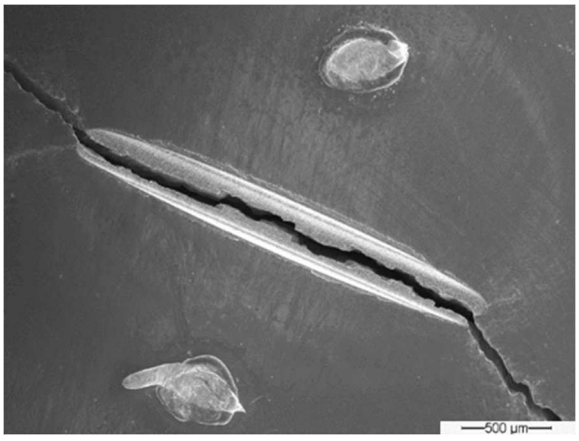

Figure 4 - Initiation and propagation of a crack from a surface imperfection at $\Delta\varepsilon_t/2 = 0.6\%$ (18MND5)

Fracture surface analysis performed by Scanning Electron Microscopy (SEM) and optical microscopy shows that multi-cracking can occur (figures 5-6). In fact, multiple micro-cracks can initiate at different locations along the notch root and quickly coalesce to form a single crack encompassing the entire length of the notch root. Such an example of multi-cracking is given in figure 5 with the first ink marking represented in this figure with the dotted line and corresponding to an advancement of 3% in the lifetime. First, as illustrated in figure 6, the river lines on the fracture surface demonstrate that there is not a single initiation site since they do not converge to a specific location, but rather seem to originate from several locations along the imperfection root. Moreover, striations visible in figure 6.a exhibit different propagation directions, which also suggest the presence of several initiation positions. In some cases, multi-cracking has been observed with the formation of cracks in distinct planes. Nevertheless, this phenomenon could not be associated with a particular surface condition. Furthermore, it should be noticed that, irrespective of the test conditions, the imperfection edges do not appear as privileged initiation sites.

Finally no significant differences in the crack initiation mode have been identified according to the defect type. Only the imperfection flanks differ with the presence of microcracks on EDM ones (figure 6.b) in contrast to abrasive-type defects which do not display any sign of damage.

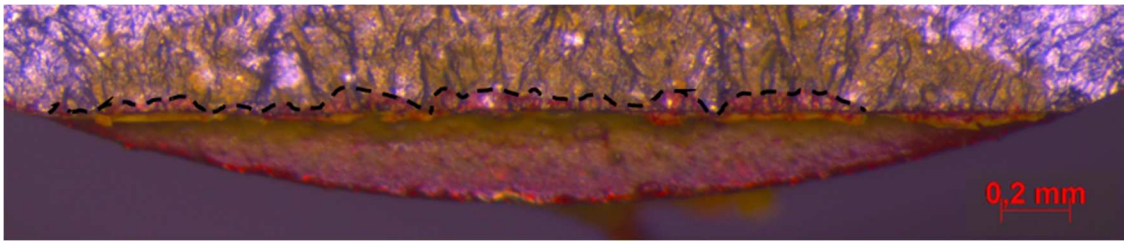

Figure 5 - Optical microscopy example of crack initiation from fracture surface presenting ink markings - Initial surface imperfection made by EDM (Depth = 280 µm, $\Delta\varepsilon_t/2 = 0.6\%$; 304L)

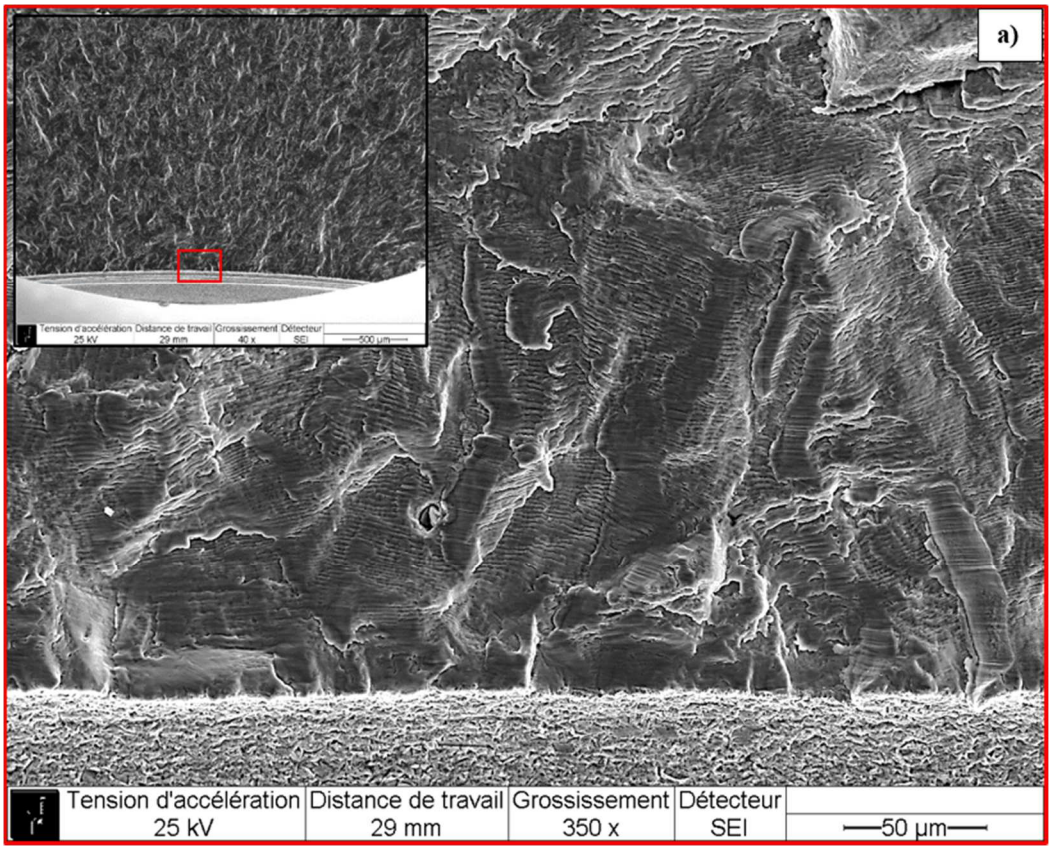

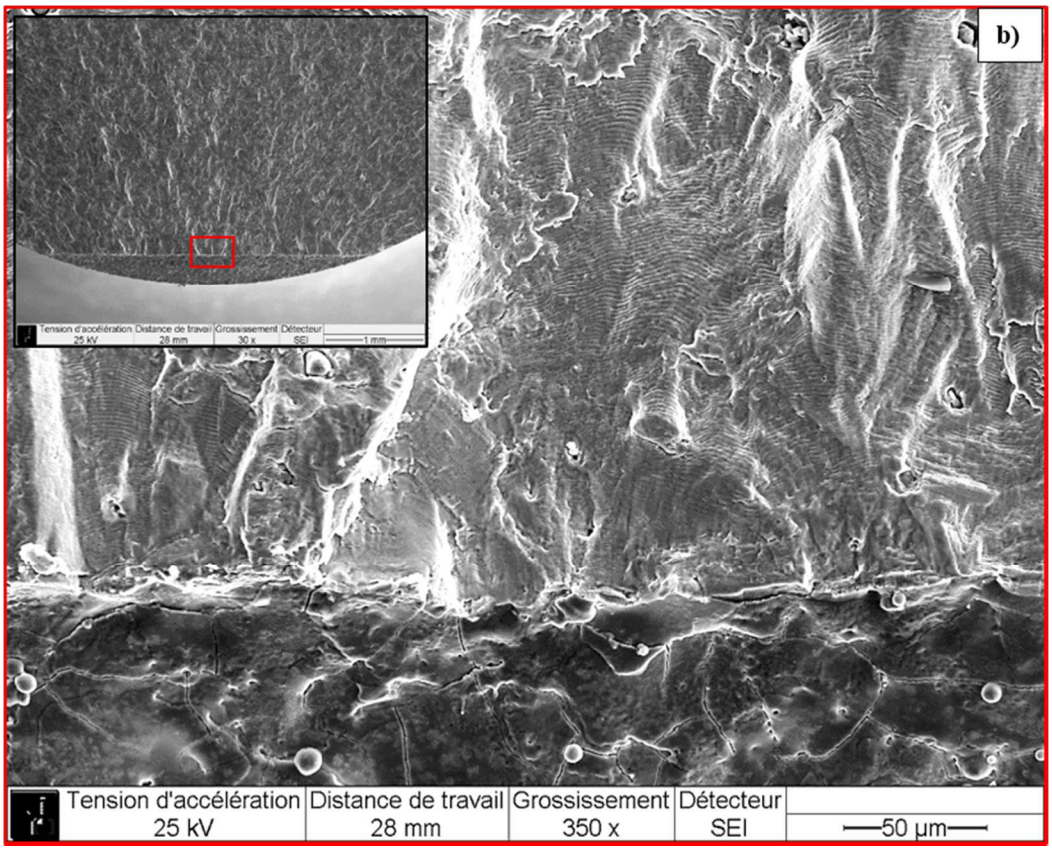

Figure 6 - 304L fracture surface analysis by SEM - a) Potential initiation site from abrasive machine imperfection ; b) potential initiation site from EDM imperfection

3.2.2. Crack initiation stage

All experimental data obtained from the electrical potential monitoring have been analyzed using the previously defined threshold value associated with a crack propagation distance of about 100 µm ($V/V_0 = 1.01$). For each test performed, this allows to assess the crack initiation duration, called $N_{initiation}$. The results obtained for both 304L and 18MND5 steels at the different strain amplitudes are listed in table 3. The fatigue lifetime of each specimen is also recorded in this table. The lifetime considered here, noted N_5, corresponds, as mentioned in the section 2.2, to a 5% decrease from the stabilized stress.

Material	$\Delta\varepsilon_t/2$	Imperfection type	Imperfection depth (micrometers)	N_5 (cycles)	$N_{initiation}$ (cycles)	Proportion of crack initiation
304L	0.2%	EDM	110	19 100	2 800	15%
		Abrasive machine	110	27 300	6 500	24%
		Abrasive machine	220	16 610	1 120	7%
		EDM	320	10 200	400	4%
		Abrasive machine	320	12 000	1 000	8%
	0.3%	Abrasive machine	120	7 710	910	12%
		Abrasive machine	180	7 550	1 280	17%
		Abrasive machine	350	3 800	290	8%
	0.6%	Abrasive machine	110	1 750	300	17%
		EDM	170	1 500	220	15%
		EDM	280	910	30	3%
		Abrasive machine	280	970	110	11%
		Abrasive machine	290	910	70	8%
		EDM	310	840	80	10%
18MND5	0.2%	Abrasive machine	50	66 900	21 810	33%
		Abrasive machine	140	42 940	2 580	6%
		Abrasive machine	270	19 150	1 510	8%
	0.6%	Abrasive machine	130	1 010	70	7%
		Abrasive machine	220	620	90	15%
		Abrasive machine	330	610	60	10%

Table 3 - Fatigue lifetimes and initiation duration for 304L and 18MND5 steels

In the case of the 304L steel, whatever the strain level considered, the fraction of the total life consumed during crack initiation is relatively small in the presence of a surface imperfection. The proportion of crack initiation in the total lifetime varies from 3 to 24% maximum. Regardless of the imperfection depth, it can also be noticed that the strain amplitude, as expected, plays a major role on initiation duration in absolute value, the latter decreasing sensibly when the strain level increases. Furthermore, the influence of the imperfection depth and type can be noted. Indeed, the number of cycle to initiation tends to decrease along with the increase in crack depth. As an example, at $\Delta\varepsilon_t/2 = 0.6\%$, $N_{initiation} = 300$ cycles for an initial imperfection depth of 110 µm while it represents only 90 cycles for a 290 µm initial depth. One can notice that in some cases, this trend is not always respected, especially when the imperfection type considered differs. Actually, at equivalent depths and strain amplitude, the EDM type imperfections can be associated with lower initiation times. The influence of the imperfection type and depth on the 304L steel is discussed in particular in the section 4.1.

In the case of the 18MND5 steel, the initiation in the presence of imperfection represents between 6 and 33% of the total lifetime N_5. As for the stainless steel, the initiation times are

strongly reduced in absolute value for the higher applied strain amplitude. However, when considering the proportion of crack initiation, the results does not exhibit any significant effect of the strain amplitude. Besides, an analysis of the data according to the crack depth shows that, in the frame of the depth considered for this material, this latter parameter does not have a particular impact on the crack initiation execpt for the lowest depth, namely 50 µm. Actually, in a depth interval included between 130 and 330 µm, the relative crack initiation times remain close to 10% and vary only from 6 to 15%. This result suggests that from a certain depth level, no significant changes in the proportion of crack initiation should be expected on this material.

Eventually, in the presence of a surface imperfection, regardless of its depth or type, cracks initiate very rapidly, meaning that most of the fatigue lifetime is represented by the propagation stage. The analysis of this phase is therefore of particular importance and is addressed in the next sections.

3.3. Fatigue crack propagation analysis

3.3.1. Crack front shape evolution

The fracture surface observations have also enabled to reconstruct the crack propagation history from surface imperfections by analyzing ink markings and crack front shapes corresponding to the end of the tests. After the initiation stage described in the previous section, it is noticed that the crack front quickly evolves into a semi-elliptical shape that can be described by two characteristic parameters *a* and *b*. Figure 7 introduces the convention that was adopted during this study to analyze the crack shape evolution. The quantity *a* corresponds to the crack depth measured from the specimen surface to point C (this distance is also called semi-minor axis of the ellipse) and *b* is assimilated to the semi-major axis, then, *a/b* is the ellipticity ratio.

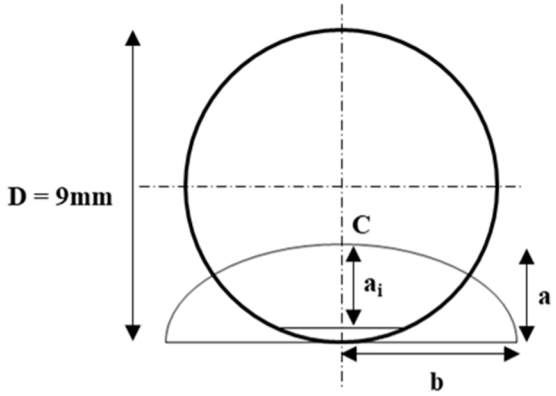

Figure 7 - Semi-elliptical crack front characterized by the parameters *a* (crack depth from the surface) and *b* (semi-major axis of the ellipse) ; a_i (crack depth from the notch root)

Case of 304L

For 304L, during crack propagation, the crack front retains a semi-elliptical shape. It starts with an elongated shape (low *a/b* ratio) and then evolves towards a circular one (*a/b* increases) before stabilizing around a shape having an ellipticity ratio close to 0.7. Figure 8 shows the evolution of this ratio as a function of the dimensionless value *a/D* (crack depth *a* divided by the specimen diameter *D* whose value is 9 mm). The analysis of the experimental points presented in figure 8 according to the applied strain amplitude or the initial defect depth demonstrates that these two parameters have no influence on the crack front shape evolution. However, given the relatively limited number of data points and the analysis of fracture surfaces, the crack front

shape may slightly differ from one defect to another one in the early stages of propagation. Indeed, during the initiation and the beginning of micropropagation stage, the hypothesis of a semi-elliptical crack is not valid. As shown in the previous section (figure 5), the crack does not immediately satisfy the semi-elliptical crack shape assumption, with an initial irregular shape. Thus, the very first points in figure 8 must be considered with care as, in this propagation domain, the assumption of a semi-elliptical crack is not fully consistent with experimental observations.

Beyond initiation and early stages of propagation, generally, once the crack has begun to propagate on the specimen edge, getting out of the initial defect, the semi-elliptical crack front assumption is systematically respected, and the influence of the initial defect appears to be negligible. This result is also consistent with literature data from Carpinteri [26]. This author has actually modeled the crack front shape evolution in a round bar from initial cracks presenting different geometric characteristics. The conclusions from Carpinteri highlight a convergence of the crack shape towards an *a/b* ratio close to 0.6 independently of the initial conditions, in consistency with the results presented here.

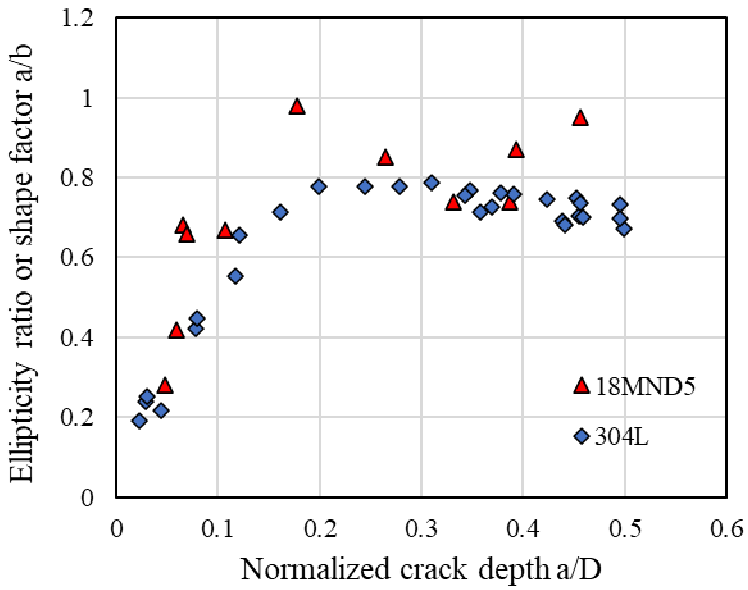

Figure 8 - Evolution of the *a*/b ratio determined experimentally from the fracture surfaces analysis for both 304L and 18MND5 steels

Case of 18MND5

Despite a relatively large scatter, the evolution of the crack front shape in 18MND5 steel is similar to the one observed in 304L steel. Thus, after initiation, the crack front, which has an initially elongated shape, rapidly evolves into a more circular one. A few points deviate however from the general trend and correspond with values of the *a/b* ratio close to 1. The discrepancy observed could be attributed to the crack deflection systematically observed on the sample surfaces. One example of such crack deviation upon the specimen barrel is shown in figure 9. Actually, the crack front shape considered for the determination of the *a/b* ratio corresponds to a projection onto a propagation plane viewed as perpendicular to the loading axis. The consideration of the real crack front would tend to increase the value of the semi-major axis *b* and consequently to decrease the one of the *a/b* ratio which would thus become closer to those observed on the 304L steel. Moreover, a topographic analysis has been

performed (figure 9) and shows that the deflection is only effective in the immediate vicinity of the specimen edges and, in the fracture surface center, the crack lips remain flat. Eventually, while the crack deflection could potentially explain the particular crack front shape recorded on this material, further investigations should be undertaken in order to validate or not this hypothesis and understand the origin of this phenomenon.

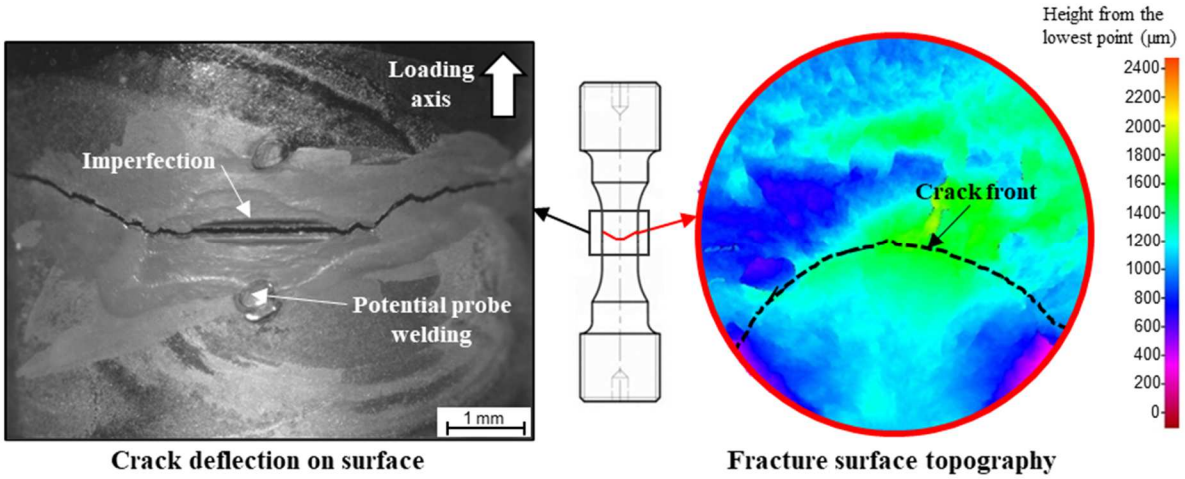

Figure 9 - Illustration of the crack deflection occurring on 18MND5 steel specimens - Crack deflection at the specimen surface (on the left) ; Topographic analysis by optical microscopy of the fracture surface (on the right)

3.3.2. Fatigue crack growth rates derived from DCPD measurements

The fatigue crack growth rates derived from the electrical potential tracking analysis using the calibration curve previously established are represented as a function of the crack depth in figure 10, for the various strain amplitudes studied.

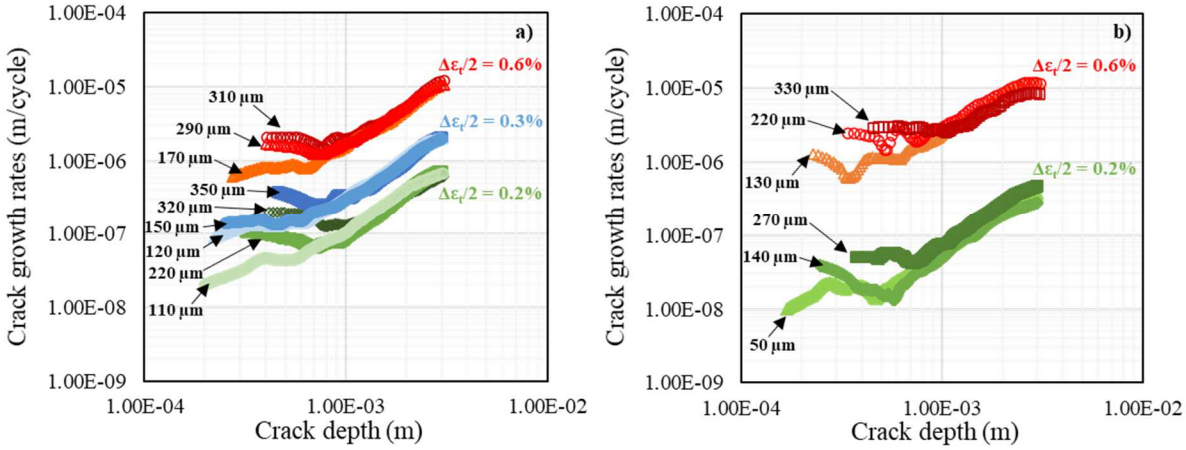

Figure 10 – Fatigue crack growth rates as a function of crack depth - a) 304L ; b) 18MND5 (Initial imperfection depths are indicated with arrows)

Case of 304L

The crack propagation rates appear to be strongly dependent on the strain level as shown in figure 10.a. Indeed, for a total strain amplitude of 0.2%, fatigue crack propagation rates range from 2×10^{-8} to 7.2×10^{-7} m/cycle while at $\Delta\varepsilon_t/2 = 0.3\%$ strain level, they range from 1×10^{-7} to

2×10^{-6} m/cycle and at last, they vary from 4×10^{-7} to 1.5×10^{-5} m/cycle at the highest strain level $\Delta\varepsilon_t/2 = 0.6\%$.

Regardless of the strain amplitude or the imperfection depth considered, the evolution of fatigue crack propagation rates can be systematically divided into two parts. Thus, in the first part of the curves corresponding to depths from the initiation threshold to depths varying approximately between 0.6 and 1.3 mm maximum (according to the initial imperfection), the crack propagation rates present a pseudo-plateau behaviour, with a relatively small increase, or even a decrease, and undergo significant fluctuations. Moreover, this propagation domain seems to be very dependent on the initial imperfection depth. Indeed, the deeper the initial notch is, the higher the initial crack propagation rates are.

Beyond a certain threshold in terms of crack depth, which seems to depend on the imperfection depth considered, fatigue crack propagation rates from different tests tend to merge along a unique curve, which will be associated here to a steady-state crack propagation regime. In this domain, the increase in crack growth rates as a function of crack depth is independent of both strain amplitude and initial imperfection depth and seems to evolve as a power-type function. At the end of the curves, one can notice a slope change which is characterised by a reduction in the rate of increase. This effect can be attributed to the significant damage present in the specimen at the end of the test, contributing significantly to its deformation and leading to crack driving force drop.

Case of 18MND5

In the low alloy steel 18MND5, fatigue crack propagation rates are once again controlled by the strain amplitudes: an increase in the strain amplitude leads to a substantial increase in crack growth rates. At $\Delta\varepsilon_t/2 = 0.2\%$, crack propagation rates observed range from about 1×10^{-8} to 5×10^{-7} m/cycle while the range is from 1×10^{-6} to 1×10^{-5} m/cycle at $\Delta\varepsilon_t/2 = 0.6\%$.

As for 304L material, two propagation stages can be observed on this material, regardless of the strain level considered. Once again, the first propagation stage is characterized by a strong dependence on the initial imperfection depth and is still associated with significant fluctuations. The dependency of growth rates on initial surface imperfections also follows the same trend as observed on the 304L: the initial fatigue crack propagation rates increase with the imperfection depth. Above a threshold (comparable with the ones observed on the 304L), also depending on the notch depth, a change in the propagation regime occurs. The crack growth becomes independent of the initial imperfection and is only governed by the applied strain amplitude. In the same way, as for the stainless steel and for similar reasons, a drop in the crack driving force can also be observed at the end of the curves.

Crack growth rate comparison between 304L and 18MND5

A comparison of the evolution of fatigue crack propagation velocities for 304L and 18MND5 steels is proposed in figure 11. Crack growth rates associated with 304L steel are higher than those of 18MND5 at $\Delta\varepsilon_t/2 = 0.2\%$ on the whole propagation range. However, the differences are particularly marked in the micropropagation domain. For the highest strain level, at $\Delta\varepsilon_t/2 = 0.6\%$, the growth rates are generally very close, although those associated with stainless steel appear to be slightly lower.

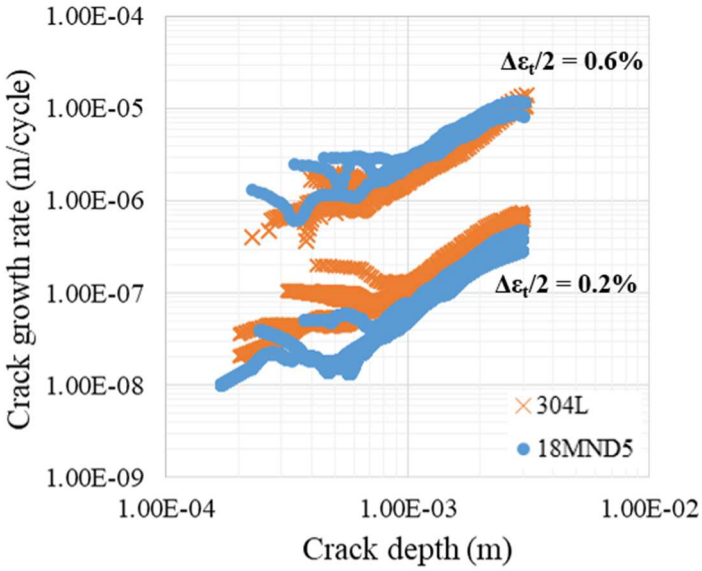

Figure 11 - Comparison of both 304L and 18MND5 crack growth rates derivated from potential monitoring analysis at $\Delta\varepsilon_t/2 = 0.2\%$ and $\Delta\varepsilon_t/2 = 0.6\%$

The important differences in velocities observed at $\Delta\varepsilon_t/2 = 0.2\%$, especially in the first propagation domain, are partly linked to the highly dissimilar plasticity levels at this strain amplitude between these two steels. Indeed, the higher crack propagation rates on the 304L could derived from the significant plasticity occurrence at low strain amplitude, contrary to the 18MND5 (figure 12). This generalized plasticity is likely to assist the crack propagation and thus to promote higher velocities.

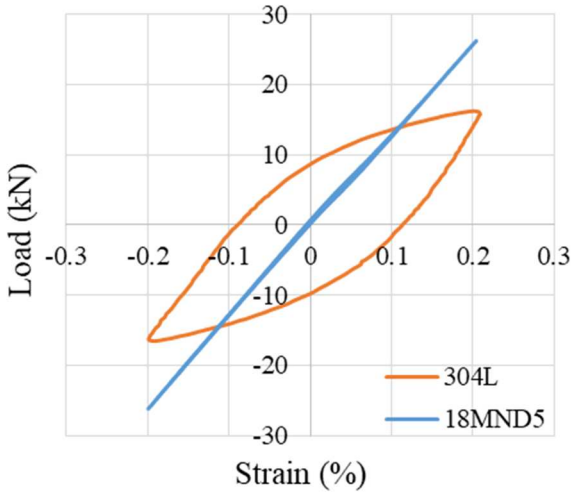

Figure 12 - Comparison of 304L and 18MND5 hysteresis loop at $\Delta\varepsilon_t/2 = 0.2\%$

3.4. Influence of surface imperfections on fatigue strength

In this section, the influence of surface imperfections on the fatigue strength is studied through an analysis of the relative lifetime evolution as a function of the initial defect depth. The relative lifetime corresponds to the ratio of the lifetime in the presence of a defect to the reference lifetime associated with virgin specimens. The fatigue lifetimes considered here are the previously defined N_5 lifetime and the lifetimes derived from the ANL (Argonne National

Laboratory) equations presented below. Indeed, in the framework of this study, only one reference test (without imperfection) has been performed for each strain amplitude, the use of ANL equations as reference allows to overcome the natural scatter which may be associated to these tests. The ANL fatigue lives, noted here N_{ANL}, are provided from equations 1 and 2 for the low alloy steels and from equations 3 for the austenitic stainless steels. These equations are derived from fatigue life models for estimating the fatigue lives in air based on the existing fatigue ε-N data at ANL as best-fits of a Langer curve to the data [27].

Equations 1 and 2 provide the ANL fatigue life for low alloy steel in air at a given temperature T:

$$\ln(N_{ANL}) = 6.480 - 0.00124T - 1.808\ln(\varepsilon_a - 0.151) \quad (1)$$

Thus, in room temperature the equation (1) is expressed as:

$$\ln(N_{ANL}) = 6.449 - 1.808\ln(\varepsilon_a - 0.151) \quad (2)$$

Equation 3 gives the ANL fatigue life for austenitic stainless steel in air at temperatures up to 400°C:

$$\ln(N_{ANL}) = 6.891 - 1.92 \times \ln(\varepsilon_a - 0.112) \quad (3)$$

Where N_{ANL} is the fatigue life in cycles, ε_a the strain amplitude and T the test temperature (°C).

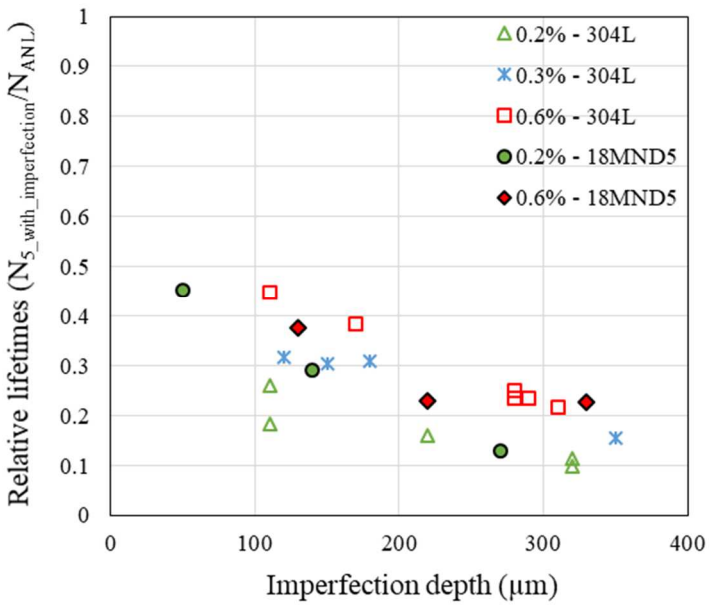

Figure 13 - Evolution of the relative lifetime as a function of imperfection depth for 304L and 18MND5

Regardless of the material or strain amplitude considered, it can be seen in figure 13 that fatigue life is strongly affected by the presence of a surface imperfection. Indeed, even in presence of shallow imperfections whose depths are close to 50 or 100 µm, a significant reduction in fatigue strength is noticed. Furthermore, the results presented in figure 13 highlight the influence of the imperfection depth which appears to be the main parameter governing the fatigue life. The analysis of lifetime evolution as a function of other geometric parameters such as the opening angle or the notch tip radius does not reveal any particular trend whatever the material or strain level considered. This result is consistent with the works of several authors [3,5] who have studied the influence of surface imperfection such as scratches.

Besides, the data analysis associated with the 304L steel also suggests that the surface imperfection effect on fatigue strength could depend on the strain amplitude. Actually, at equivalent depth, the presence of a surface imperfection seems to be more harmful at low strain levels, especially for the lowest value, $\Delta\varepsilon_t/2 = 0.2\%$. In the low alloy steel 18MND5, no particular influence of the strain level can be put forward in the limited data set.

The comparative analysis in figure 13 does not evidence any particular difference in the sensitivity of these two steels to the presence of imperfections. In fact, their influence does not seem, in the test conditions examined, to be more pronounced in either of the two materials, despite of their difference in microstructure and associated mechanical properties. Nevertheless, a closer look at the results according to the strain amplitudes indicates that 18MND5 could be slightly less sensitive to the presence of imperfection at the lowest strain level, namely $\Delta\varepsilon_t/2 = 0.2\%$. Indeed, for the first two points, associated with depths of 50 and 140 µm, the relative lifetimes appear to be higher than those that would be obtained, at equal depths, on 304L. This difference between the two materials could possibly come from the radically different amount of cyclic plasticity generated for a given total strain amplitude (see figure 12). The aforementioned trends regarding the 18MND5 steel should nevertheless be considered cautiously due to the limited number of experimental points available for this material.

4. Discussion

4.1. Crack initiation from surface imperfection

It has previously been shown (section 3.2.2) that the imperfection depth and type of machining (abrasive machine and EDM) can affect the initiation durations. An analysis of the proportion of fatigue life devoted to crack initiation, represented by the ratio $N_{initiation}/N_5$, as a function of the initial imperfection depth is provided for both 304L and 18MND5 in figure 14. Results are also distinguished according to the imperfection type (EDM or abrasive machine).

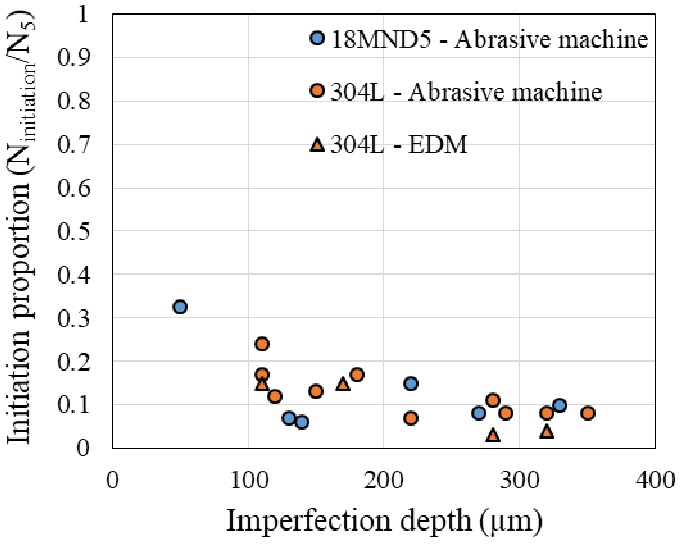

Figure 14 - Evolution of the relative crack initiation time according to the initial imperfection depth

For the two materials studied here, figure 14 illustrates that the relative initiation times tend to decrease with the rise of the surface imperfection depth. In the 304L steel, for imperfections whose depths are close to 100 µm, the proportion of crack initiation lifetime varies from 15 to 24%, while it ranges from 3 to 11% for imperfections with depths close to 300 µm. The variations observed in this material at equivalent depths may be due to the type of imperfection. Indeed, the electroerosion process seems to favour a faster initiation compared to the abrasive machine. Two reasons can mainly be put forward to explain these differences between the two imperfection types. First, the surface finish associated with EDM-type imperfections has a much more pronounced roughness than the one observed on abrasive machine imperfections (figure 15). Some studies, conducted on 304L steel [8-9], have demonstrated the significant effect of this parameter on fatigue crack initiation. In addition, because of its nature and unlike the abrasive machine, the electroerosion process strongly interacts with the material by creating a heat-affected zone which may also contribute to a faster initiation. Finally, the use of copper electrodes for machining EDM-type imperfections can potentially induce local copper contamination which could also influence the crack initiation resistance. Nevertheless, BSE (Back Scattering Electron) analyses performed on one of the defects did not reveal any particular chemical constituent which tends to exclude this hypothesis.

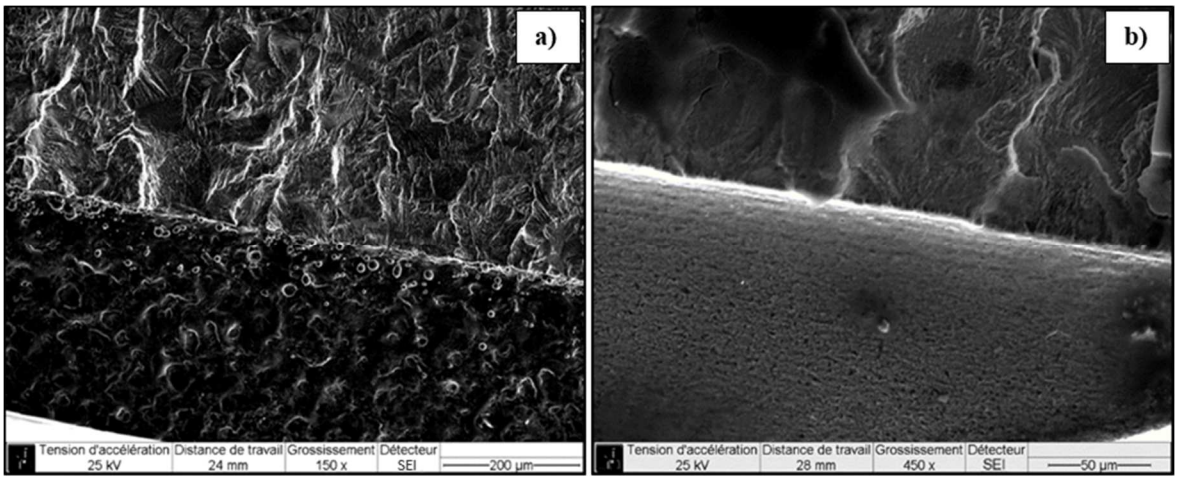

Figure 15 - Surface imperfection roughness - a) EDM ; b) Abrasive machine

Furthermore, a comparison of the 304L initiation results with literature data has been carried out. As expected, initiation times appear to be significantly reduced in the presence of surface imperfection when compared with virgin specimens [7, 28]. For the strain amplitudes considered here, it appears that initiation represents an important part of the total fatigue life. A recent study [7] conducted under air at room temperature confirms the impact of the presence of a surface imperfection on crack initiation. As an example, the fraction of the lifetime represented by initiation for specimens without imperfection is respectively 32% and 31% at $\Delta\varepsilon_t/2 = 0.2\%$ and 0.3%. It should be noted that the initiation proportion is significantly lower at $\Delta\varepsilon_t/2 = 0.6\%$, reaching only 8 to 15% of the total lifetime. However, these results are not directly comparable with those of the present study. Indeed, in Ould Amer's work [7], initiation is associated with the nucleation of a crack with a 100 µm surface length while the initiation as defined in this study is associated to a depth of 100 µm. A 100 µm surface crack length is associated with a depth which obviously depends on the crack front shape, but which is very likely less than 100 µm (see figure 8). Thus, the initiation proportion from Ould Amer's work

mentioned above would probably be higher if the same initiation criterion, i.e. the nucleation of 100 µm-depth crack, were considered.

4.2. Short crack effect and steady-state propagation threshold

The distinction of a micropropagation phase presenting a different fatigue crack growth rate evolution that the one observed for long cracks is a well-known phenomenon in fatigue. The propagation of so-called short cracks has been the subject of numerous studies. Their particular behavior compared to long cracks is generally attributed to miscellaneous factors such as microstructure, environment or again crack closure [29]. In austenitic stainless steels, this phenomenon has been investigated by several authors [7, 19, 20, 30, 31]. Some of them [7, 19, 20] have highlighted the presence of a short crack propagation stage in large scale yielding conditions. These latter studies have been carried out on flawless specimens in contrast to the present study. There is therefore a "short crack" effect, independently of the presence of imperfections. In his study on the 304L, Ould Amer [7] has distinguished three propagation domains: the first two ones, corresponding respectively to the microstructural and physical short cracks evolution, can be associated with the micropropagation stage while a third domain is assimilated to the propagation of long cracks. During the first two propagation stages, the author shows a significant fluctuation in the propagation rates. The particular crack evolution in this micropropagation phase is attributed to microstructural effects. The grain boundaries and grain orientation are identified as the main causes of the observed crack growth fluctuations. Actually, grain boundaries act as microstructural barriers that can cause significant deceleration. Strong disorientation between adjacent grains can also lead to a decrease in the propagation rate.

In the context of this study, in addition to the above-mentioned microstructural effects, it has been clearly shown that the micropropagation domain is strongly dependent on the surface imperfection presence. Actually, the strain concentration induced by the surface imperfections seems to influence the propagation rates during the micropropagation phase as it has been described in the results section. Moreover, in this propagation domain, the crack growth rate could also be affected by multi-cracking phenomena previously mentioned. It has been shown (figure 5) that, in the early stages of propagation, the crack front shape is irregular and it adopts a semi-elliptical shape mainly after propagating from the initial surface imperfection edge. Then, the emergence of the steady-state propagation regime previously defined may be linked with the end of multi-cracking and coalescence phenomena and the presence of a fully semi-elliptical crack. Estimations from crack growth rates data have been performed on both 304L and 18MND5 in order to identify the appearance of the steady-state propagation regime. The results are presented in figure 17 and compared with the evolution of the crack depth when it separates from the initial surface imperfection. This characteristic crack depth, which will be called “transition depth” here for simplicity sake, is based on the experimental data related to the crack front shape evolution. This “transistion crack depth” concept is illustrated in figure 16.

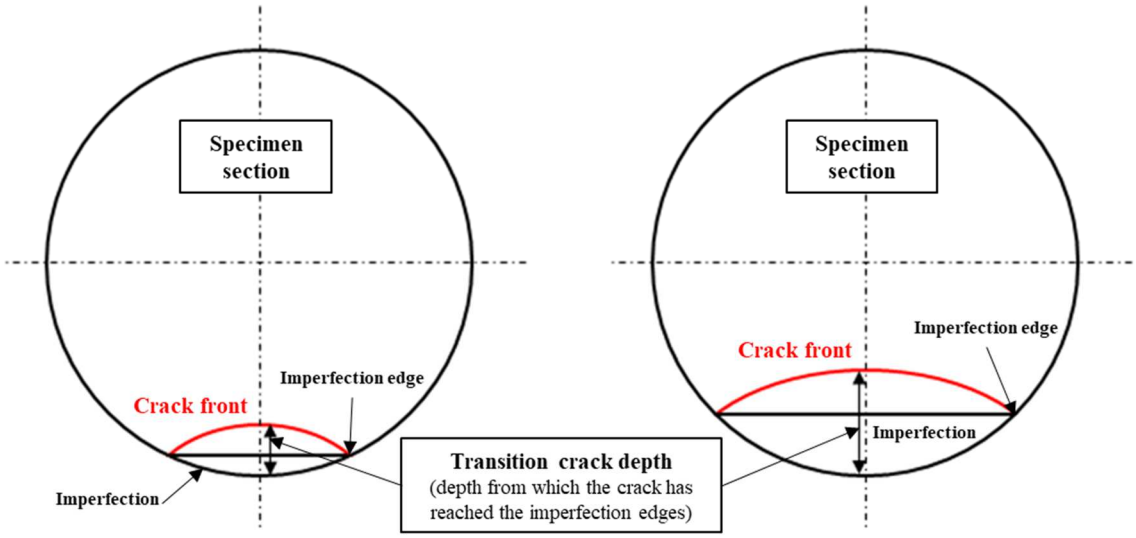

Figure 16 - Schematic illustration of the "transition crack depth" (two examples shown with different initial imperfection depths)

The comparison between the steady-state propagation threshold and the transition depth suggests that these parameters could be potentially linked to each other. Moreover, the correlation between the data from the two materials seems to indicate that the particular evolution of the fatigue crack growth rates and the steady-state regime onset are rather mechanically-driven than microstructurally controlled. Indeed, the microstructures of the two steels considered in this study are fundamentally different.

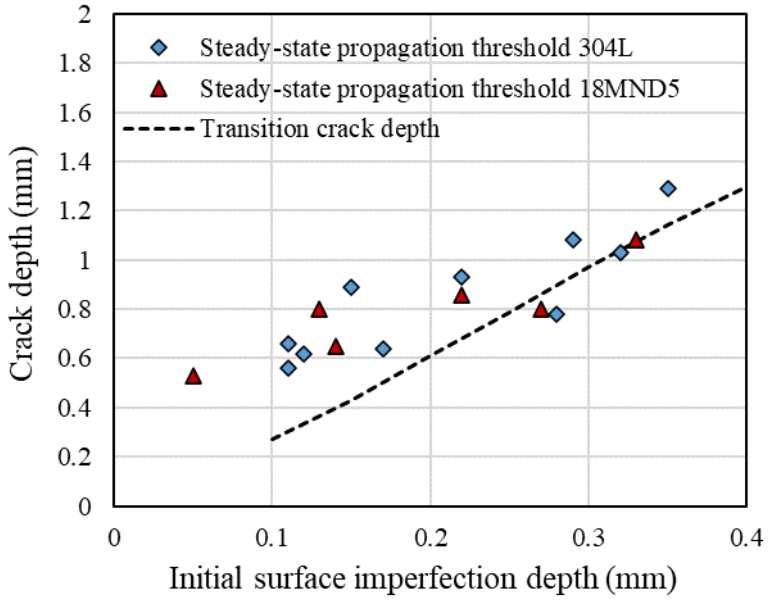

Figure 17 - Comparison of the evolution of the steady-state propagation regime threshold for 304L and 18MND5 steels as a function of the initial imperfection depth with the evolution of the "transition crack depth" evolution

Conclusions

The influence of the presence of surface imperfections on the fatigue strength of two steels has been studied here on the basis of uni-axial fatigue tests carried out in total strain amplitude control. A particular attention has been paid to assess the respective contribution of crack initiation and propagation from the artificially introduced imperfections in the observed fatigue life by implementing the electrical potential monitoring method in order to quantify the initiation durations and the crack growth rates.

The main results can be summarized as follows :

- The analysis of crack initiation in the 304L, with respect to the threshold criterion defined in the present study (1% variation of $V/V_0 \approx 100$ µm crack), has shown that in the presence of imperfection, the propagation stage represents the main part of the fatigue life. The exploitation of the data for the 18MND5 steel confirms this statement. In addition, for the 304L, the proportion of initiation is dependent on the initial imperfection depth, in particular at lower strain amplitudes. This latter result is not clearly evidenced for the low alloy steel.
- An analysis of the fatigue crack propagation rates, derived from electrical potential monitoring, has been proposed. Two propagation domains were distinguished: a first one, assimilable to the micropropagation phase previously defined between the initiation threshold and depths varying approximately between 0.6 and 1.3 mm. This phase is strongly dependent on the initial surface imperfection. The second stage, qualified as a steady-state regime, is characterised by a regular evolution independent on the initial conditions, especially the imperfection depth.
- Concerning the fatigue lifetime, the results indicate that the presence of surface imperfections induces a significant reduction in fatigue life, even for shallow depths close to 100 µm. The imperfection depth appears to be the main parameter governing the fatigue life. Finally, the fatigue life abatements are due to a combination of two phenomena, first, a systematic reduction in crack initiation and secondly, the high crack growth rates in the micropropagation stage especially for the deepest imperfections.

Experimental data obtained in the framework of this study on crack initiation and propagation should now be further exploited in view of the proposal of a predictive method. In particular mechanical parameters such as ΔJ or ΔK_ε [32-33], which can be used in the context of large-scale plasticity of this work, will be considered as driving force parameters to analyze the fatigue crack growth data from the different tests.

Acknowledgements

The author acknowledges the Région Nouvelle-Aquitaine as well as the Framatome company for their financial support. Special thanks are also extended to the entire laboratory technical staff of the Pprime ENDO group for their assistance during the fatigue tests as well as for the specimen preparation.

References

[1] Doremus, L., Cormier, J., Villechaise, P., Henaff, G., Nadot, Y., Pierret, S., 2015a. Influence of residual stresses on the fatigue crack growth from surface anomalies in a nickel-based superalloy. Mater. Sci. Eng. -Struct. Mater. Prop. Microstruct. Process. 644, 234–246. https://doi.org/10.1016/j.msea.2015.07.077

[2] Gourdin, S., Cormier, J., Henaff, G., Nadot, Y., Hamon, F., Pierret, S., 2017. Assessment of specific contribution of residual stress generated near surface anomalies in the high temperature fatigue life of a Rene 65 superalloy. Fatigue Fract. Eng. Mater. Struct. 40, 69–80. https://doi.org/10.1111/ffe.12475

[3] Cini, A., Irving, P.E., 2010. Transformation of defects into fatigue cracks; the role of Kt and defect scale on fatigue life of non-pristine components. Procedia Eng. 2, 667–677. https://doi.org/10.1016/j.proeng.2010.03.072

[4] Jiang, Q., Sun, C., Liu, X., Hong, Y., 2016. Very-high-cycle fatigue behavior of a structural steel with and without induced surface defects. Int. J. Fatigue 93, 352–362. https://doi.org/10.1016/j.ijfatigue.2016.05.032

[5] Inchekel, A., Talia, J.E., 1994. Effect of scratches on the fatigue behavior of an Al-Li alloy. Fatigue Fract. Eng. Mater. Struct. 17, 501–507

[6] De Baglion, L., Mendez, J., 2010. Low cycle fatigue behavior of a type 304L austenitic stainless steel in air or in vacuum, at 20 °C or at 300 °C: Relative effect of strain rate and environment. Procedia Eng., Fatigue 2010 2, 2171–2179. https://doi.org/10.1016/j.proeng.2010.03.233

[7] Ould Amer, A., 2014. Endommagement à différentes échelles d'un acier austénitique inoxydable en fatigue à amplitude constante et variable. ENSTA ParisTech

[8] Poulain, T., Mendez, J., Hénaff, G., de Baglion, L., 2017. Analysis of the ground surface finish effect on the LCF life of a 304L austenitic stainless steel in air and in PWR environment. Eng. Fract. Mech. 185, 258–270. https://doi.org/10.1016/j.engfracmech.2017.05.043

[9] Petitjean, S., 2003. Influence de l'état de surface sur le comportement en fatigue à grand nombre de cycles de l'acier inoxydable austénitique 304L. Thèse de l'Université de Poitiers

[10] Clark, G., Knott, J.F., 1975. Measurement of fatigue cracks in notched specimens by means of theoretical electrical potential calibrations. J. Mech. Phys. Solids 23, 265–276

[11] Johnson, H.H., 1965. Calibrating the Electric Potential Method for Studying Slow Crack Growth. Mater. Res. Stand. 5, 442

[12] Smith, R.A., Cameron, A.D., 1984. A three dimensional wax analogue for the calibration of the electrical potential technique of crack growth monitoring, in: Valluri, S.R., Taplin, D.M.R., Rao, P.R., Knott, J.F., Dubey, R. (Eds.), Fracture 84. Pergamon, pp. 3371–3376. https://doi.org/10.1016/B978-1-4832-8440-8.50362-8

[13] Ritchie, R.O., Bathe, K.J., 1979. On the calibration of the electrical potential technique for monitoring crack growth using finite element methods. Int. J. Fract. 15, 47–55

[14] Gandossi, L., Summers, S.A., Taylor, N.G., Hurst, R.C., Hulm, B.J., Parker, J.D., 2001. The potential drop method for monitoring crack growth in real components subjected to combined fatigue and creep conditions: application of FE techniques for deriving calibration curves. Int. J. Press. Vessels Pip. 78, 881–891. https://doi.org/10.1016/S0308-0161(01)00103-X

[15] Doremus, L., Nadot, Y., Henaff, G., Mary, C., Pierret, S., 2015b. Calibration of the potential drop method for monitoring small crack growth from surface anomalies - Crack front marking technique and finite element simulations. Int. J. Fatigue 70, 178–185. https://doi.org/10.1016/j.ijfatigue.2014.09.003

[16] Lambourg, A., Henaff, G., Nadot, Y., Gourdin, S., Pujol d'Andrebo, Q., Pierret, S., 2020. Optimization of the DCPD technique for monitoring the crack propagation from notch root in localized plasticity. Int. J. Fatigue 130, 105228. https://doi.org/10.1016/j.ijfatigue.2019.105228

[17] Enmark, M., Lucas, G., Odette, G., 1992. An Electric-Potential Drop Technique for Characterizing Part-Through Surface Cracks. J. Nucl. Mater. 191, 1038–1041. https://doi.org/10.1016/0022-3115(92)90632-U

[18] Ikeda, K., Yoshimi, M., Miki, C., 1991. Electrical potential drop method for evaluating crack depth. Int. J. Fract. 47, 25–38

[19] De Baglion, L., 2011. Comportement et endommagement en fatigue oligocyclique d'un acier inoxydable austénitique 304L en fonction de l'environnement (vide, air, eau primaire REP) à 300°C. Thèse Ensma, Poitiers

[20] Poulain, T., 2015. Fatigue oligocyclique d'un acier inoxydable austénitique 304L : influence de l'état de surface et de signaux de chargement en milieu eau primaire REP

[21] Akamatsu M., Chevallier E., 2001. Caractérisation chimique et mécanique des matériaux approvisionnés pour l'étude du comportement en fatigue des aciers inoxydables austénitiques, Projet HT-42/00/020/A, EDF

[22] Ljustell, P., 2011. The Effect of Large Scale Plastic Deformation on Fatigue Crack Length Measurement with the Potential Drop Method. J. Test. Eval. 39, 985–1002. https://doi.org/10.1520/JTE103532

[23] Tarnowski, K.M., Davies, C.M., Dean, D.W., Nikbin, K.M., 2015. The Influence of Plasticity on Crack Length Measurements Using the Potential Drop Technique, in: Kang, J., Jablonski, D., Dudzinski, D. (Eds.), Evaluation of Existing and New Sensor Technologies for Fatigue, Fracture and Mechanical Testing. ASTM International, 100 Barr Harbor Drive, PO Box C700, West Conshohocken, PA 19428-2959, pp. 73–96. https://doi.org/10.1520/STP158420140055

[24] Tarnowski, K.M., Dean, D.W., Nikbin, K.M., Davies, C.M., 2017. Predicting the influence of strain on crack length measurements performed using the potential drop method. Eng. Fract. Mech. 182, 635–657. https://doi.org/10.1016/j.engfracmech.2017.06.008

[25] Maiya, P., 1979. Effects of Notches on Crack Initiation in Low-Cycle Fatigue. Mater. Sci. Eng. 38, 289–294. https://doi.org/10.1016/0025-5416(79)90134-4

[26] Carpinteri, A., 1993. Shape change of surface cracks in round bars under cyclic axial loading. Int. J. Fatigue 15, 21–26

[27] NUREG/CR-6909 Rev. 1. Effect of LWR Water Environments on the Fatigue Life of Reactor Materials

[28] Maiya, P.S., 1975. Considerations of crack initiation and crack propagation in low-cycle fatigue. Scr. Metall. 9, 1141–1146. https://doi.org/10.1016/0036-9748(75)90394-4

[29] Suresh, S., Ritchie, R.O., 1984. Propagation of short fatigue cracks. Int. Met. Rev. 29, 445–475

[30] Obrtlik, K., Polak, J., Hajek, M., Vasek, A., 1997. Short fatigue crack behaviour in 316L stainless steel. Int. J. Fatigue Vol. 19, No. 6, pp. 471–475

[31] Blochwitz, C., Jacob, S., Tirschler, W., 2008. Grain orientation effects on the growth of short fatigue cracks in austenitic stainless steel. Materials Science and Engineering A 496 59–66

[32] Dowling, N.E., 1976. Geometry effects and the J-integral approach to elastic-plastic fatigue crack growth, in: Cracks and Fracture. ASTM International

[33] Kamaya, M., 2015. Low-cycle fatigue crack growth prediction by strain intensity factor. Int. J. Fatigue 72, 80–89. https://doi.org/10.1016/j.ijfatigue.2014.11.002

Shortened version of the abstract used for the online submission

The impact of a controlled surface imperfection on the low-cycle fatigue life in two different steels is investigated. After introduction of a single imperfection with a depth varying from 50 to 350 µm in cylindrical samples, fatigue tests were conducted under fully-reversed total axial strain control in air at ambient temperature. It is shown that the fatigue life is significantly reduced, even in presence of small imperfections. In addition, the use of the potential drop methods provided an assesment of the initiation life and the determination of crack growth rates. Two characteristic crack growth domains were thus identified.